



Trait-like variants in human functional brain networks

Benjamin A. Seitzman^{a,1,2}, Caterina Gratton^{a,b,c,1,2}, Timothy O. Laumann^a, Evan M. Gordon^{d,e,f}, Babatunde Adeyemo^a, Ally Dworetzky^a, Brian T. Kraus^b, Adrian W. Gilmore^g, Jeffrey J. Berg^g, Mario Ortega^a, Annie Nguyen^a, Deanna J. Greene^{h,i}, Kathleen B. McDermott^{g,i}, Steven M. Nelson^{d,e,f}, Christina N. Lessov-Schlaggar^h, Bradley L. Schlaggar^{a,h,i,j,k,l}, Nico U. F. Dosenbach^{a,i,j,k,m,n}, and Steven E. Petersen^{a,g,i,l,n}

^aDepartment of Neurology, School of Medicine, Washington University in St. Louis, St. Louis, MO 63110; ^bDepartment of Psychology, Northwestern University, Evanston, IL 60208; ^cDepartment of Neurology, Northwestern University, Evanston, IL 60208; ^dVeterans Integrated Service Network 17 Center of Excellence for Research on Returning War Veterans, Waco, TX 76711; ^eCenter for Vital Longevity, School of Behavioral and Brain Sciences, University of Texas at Dallas, Dallas, TX 75235; ^fDepartment of Psychology and Neuroscience, Baylor University, Waco, TX 76798; ^gDepartment of Psychological and Brain Sciences, Washington University in St. Louis, St. Louis, MO 63130; ^hDepartment of Psychiatry, School of Medicine, Washington University in St. Louis, St. Louis, MO 63110; ⁱDepartment of Radiology, School of Medicine, Washington University in St. Louis, St. Louis, MO 63110; ^jKennedy Krieger Institute, Baltimore, MD 21205; ^kDepartment of Pediatrics, School of Medicine, Washington University in St. Louis, St. Louis, MO 63110; ^lDepartment of Neuroscience, School of Medicine, Washington University in St. Louis, St. Louis, MO 63110; ^mProgram in Occupational Therapy, School of Medicine, Washington University in St. Louis, St. Louis, MO 63108; and ⁿDepartment of Biomedical Engineering, McKelvey School of Engineering, Washington University in St. Louis, St. Louis, MO 63130

Edited by Michael B. Miller, University of California, Santa Barbara, CA, and accepted by Editorial Board Member Michael S. Gazzaniga September 4, 2019 (received for review February 19, 2019)

Resting-state functional magnetic resonance imaging (fMRI) has provided converging descriptions of group-level functional brain organization. Recent work has revealed that functional networks identified in individuals contain local features that differ from the group-level description. We define these features as network variants. Building on these studies, we ask whether distributions of network variants reflect stable, trait-like differences in brain organization. Across several datasets of highly-sampled individuals we show that 1) variants are highly stable within individuals, 2) variants are found in characteristic locations and associate with characteristic functional networks across large groups, 3) task-evoked signals in variants demonstrate a link to functional variation, and 4) individuals cluster into subgroups on the basis of variant characteristics that are related to differences in behavior. These results suggest that distributions of network variants may reflect stable, trait-like, functionally relevant individual differences in functional brain organization.

functional connectivity | resting-state | individual differences | networks

Identifying the nature of individual variability in human brain function is a central question in many fields of study, including psychology, psychiatry, neurology, and neuroscience. Many human neuroimaging studies have identified stable, meaningful individual differences in functional activations during task performance (1–5) or volumetric differences (e.g., refs. 6 and 7) within specific brain regions. However, a number of recent investigations have revealed substantial individual variability while subjects are at rest not only in single regions, but also in large-scale networks throughout the brain (8–16). Here, we examine the characteristics of these individual differences in brain networks, asking if they are stable and systematic features of individual brain organization. Furthermore, we investigate if the distributions of these differences within an individual have trait-like aspects that might be linked to trait-like individual differences in behavior.

Large-scale functional brain networks are composed of distributed brain areas that demonstrate correlated fluctuations in their spontaneous (resting-state) activity measured using functional magnetic resonance imaging (fMRI). Over the last decade convergent descriptions of canonical functional network organization of the human brain have emerged from fMRI studies (17, 18). These efforts have revealed that functional networks map onto known large-scale brain systems, including the motor (19), auditory (20), and visual systems (21), as well as higher-level systems, such as those for executive control (22). Furthermore, regions within the same functional network tend to coactivate during tasks (23).

Most of the aforementioned studies have analyzed data from large groups of typical adults averaged together in order to de-

lineate group-level descriptions of network organization (17, 18). However, several recent investigations have revealed variability in functional network organization across individuals (8, 9, 11, 12), including observations that highly sampled individuals show focal deviations from the group-level description (10, 13, 14). We refer to these individual-specific deviations in functional network organization as “network variants.”

Natural questions raised by the observation of variants are whether individual differences in functional brain organization relate systematically to individual differences in function. Here,

Significance

Human brain function is often studied through group-averaging, yielding valuable insight into typical organization and differences across special populations. However, cortical organization is known to vary across individuals. Here, we characterize brain regions that differ from group network organization (“network variants”). We find that network variants are present in all individuals, are stable across time within a person, and are related to functional variation in tasks. We further observe that there are separable subgroups of individuals who share common distributions of variants and differ in behavior. Our study suggests that distributions of individual differences in brain networks have a trait-like nature and sets up future investigations of their neurobiological sources and their link to stable behavioral traits.

Author contributions: B.A.S., C.G., and S.E.P. designed research; B.A.S., C.G., T.O.L., E.M.G., and S.E.P. performed research; B.A.S., C.G., T.O.L., E.M.G., M.O., and S.E.P. contributed new reagents/analytic tools; B.A.S., C.G., T.O.L., E.M.G., B.A., A.D., B.T.K., A.W.G., M.O., A.N., and C.N.L.-S. analyzed data; and B.A.S., C.G., T.O.L., E.M.G., B.A., A.D., B.T.K., A.W.G., J.J.B., M.O., A.N., D.J.G., K.B.M., S.M.N., C.N.L.-S., B.L.S., N.U.F.D., and S.E.P. wrote the paper.

The authors declare no competing interest.

This article is a PNAS Direct Submission. M.B.M. is a guest editor invited by the Editorial Board.

Published under the PNAS license.

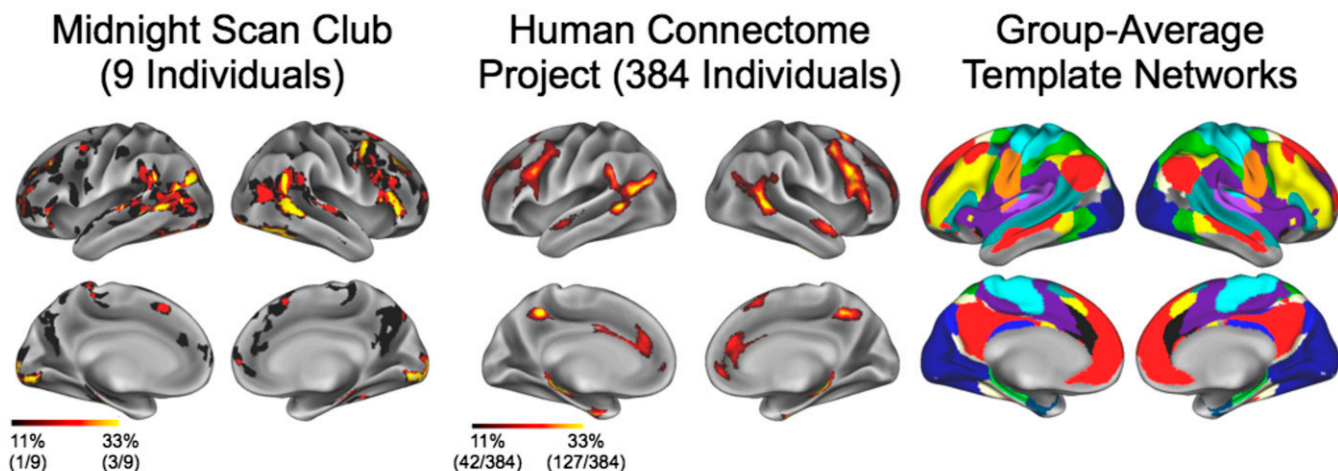
Data deposition: All data and data processing code used in the manuscript are publicly available (Midnight Scan Club and code: <https://openneuro.org/datasets/ds000224/versions/00002>; MyConnectome: myconnectome.org/wp/; Human Connectome Project: <https://db.humanconnectome.org/app/template/Login.vm>; WashU 120: <https://legacy.openfmri.org/dataset/ds000243/>). Code for network variant analyses (custom MATLAB scripts) is available at <https://github.com/MidnightScanClub>.

¹B.A.S. and C.G. contributed equally to this work.

²To whom correspondence may be addressed. Email: seitzman@wustl.edu or caterina.gratton@northwestern.edu.

This article contains supporting information online at www.pnas.org/lookup/suppl/doi:10.1073/pnas.1902932116/-DCSupplemental.

A Location of variants



B Idiosyncratic network association of variants

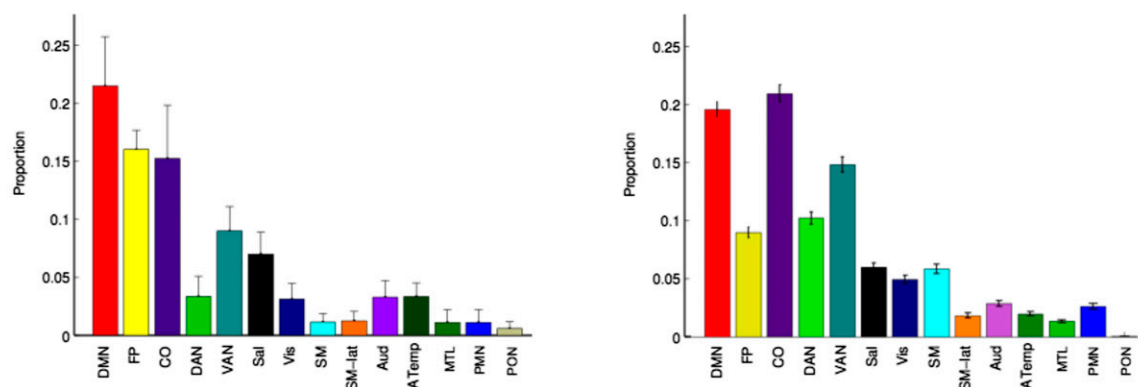


Fig. 3. Distribution of network variants across individuals. (A) The overlap of network variant locations across individuals is displayed, with brighter colors indicating increasing levels of overlap for the MSC (Left) and HCP (Center) datasets. Network variants occur commonly in lateral frontal cortex and near the temporo-occipito-parietal junction, and are rarely found in primary sensorimotor areas, the insula, superior parietal lobule, or posterior cingulate cortex. (B) In addition to occurring in characteristic locations, network variants were also typically associated with a characteristic set of networks. The mean proportion of variant functional network assignments to 14 canonical networks (12) across individuals in the MSC (Left) and HCP (Right) datasets (error bars = SEM) is displayed. A plurality of variants was assigned to the DMN (red) and CO (purple) networks across individuals in both datasets.

network variants using a data-driven approach (InfoMap) (*Materials and Methods*) (31). Given the exploratory nature of this analysis, we first examined different clustering possibilities in the MSC dataset, and then used 2 matched split-halves in the independent HCP dataset to validate the MSC results.

No clustering via anatomical location of variants. First, we examined whether individuals could be clustered according to the anatomical locations of their network variants (irrespective of functional identity). We constructed a binary map of variant locations for each subject. Then, we computed the spatial similarity of the anatomical distribution of variants between all pairs of individuals, and applied InfoMap to this spatial similarity matrix (see *Materials and Methods* for details). Across InfoMap thresholds, individuals generally grouped into a single large cluster or were unassigned to a group (e.g., for the full 384 HCP subjects the average number of individuals in the large cluster was 201 ± 130) (*SI Appendix, Fig. S8*). Thus, individuals were not classified into large subgroups of common anatomical locations of network variants.

Distinct clusters of individuals via functional network of variants. Next, we tested if individuals could be clustered according to the functional properties (network assignment) of their variants. To this end, we examined the similarity between the seed map of each

variant to standard templates of canonical functional networks (14 template functional networks were derived from a separate dataset, the WashU 120 group average; see ref. 12 for more details). This procedure produced 14 correlation coefficients per network variant, conveying the extent to which a variant is default-like, visual-like, and so forth. The mean template similarity across variants (averaged across all variants within an individual) revealed 2 distinct patterns across individuals in the MSC dataset (Fig. 5A). Importantly, we replicated the result in 2 independent, matched HCP split-halves (Fig. 5B). Again, this is notable given the differences in the subjects [e.g., IQs are much higher in the MSC dataset (13)], scanner, and acquisition parameters. Furthermore, we validated the 2-group clustering solution via a modularity-based null model as well as hierarchical clustering (*SI Appendix, Fig. S9*). The 2-subgroup solution was the most robust across datasets, with some evidence for a 4-subgroup solution (*SI Appendix, Fig. S10*).

The first subgroup consisted of individuals ($N_{\text{MSC}} = 3$ of 9, $N_{\text{HCP},1} = 92$ of 192, $N_{\text{HCP},2} = 91$ of 192) whose variants exhibited stronger correlations to the CO, DAN, and sensorimotor networks (Fig. 5, gray), suggesting that network variants in these individuals associated more strongly with control and processing

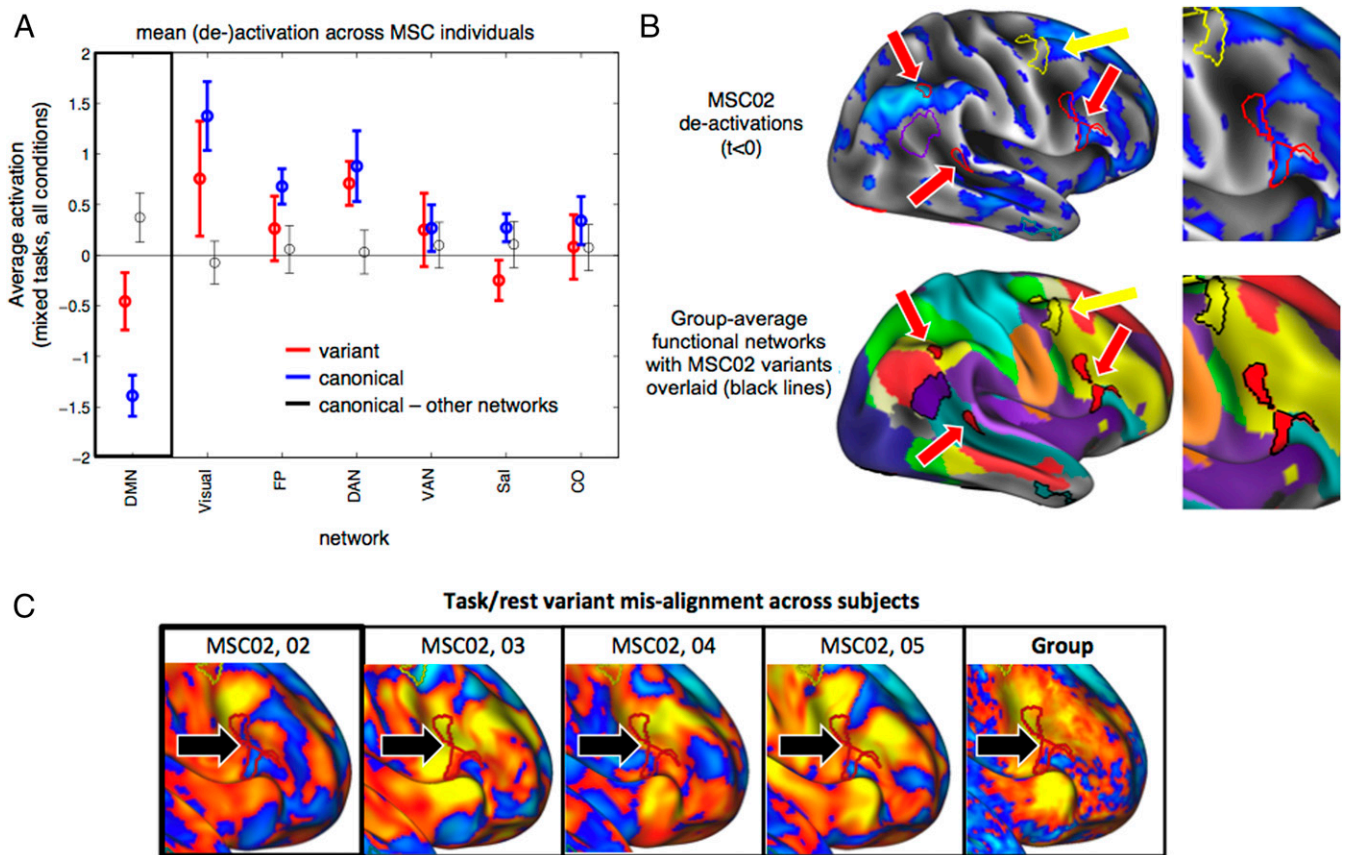


Fig. 4. Functional activation of network variants. (A) The average task-evoked activations are displayed for variants (red) assigned to different networks (x axis) and contrasted with the average activation for canonical regions in each network (blue) and for canonical regions in other networks (black). Mean de-activations are significantly stronger for DMN variants than in non-DMN canonical regions, and approach the levels of deactivation seen for canonical DMN locations (error bars = SEM across individuals). De-activations were not present across all variants; variants from task-activated networks, like visual, FP, and DAN, show activations during the task, approaching levels for canonical regions in each network. (B) Example de-activations ($t < 0$) are displayed for subject MSC02 with outlines of the individual's network variants overlaid. Note that there is strong de-activation in DMN variants (red arrows), whereas there is no deactivation in other variants (e.g., FP variant, yellow arrow). The group-average networks with the same variants overlaid are displayed below for reference, and the righthand image shows an enlarged view of 2 DMN variants in right lateral frontal cortex. (C) The same variant from MSC02 (red outline) is overlaid on an activation map from MSC02 (mostly de-activated), as well as other example subjects (MSC03-05) and the group average. In other individuals, this location exhibits activations. Indeed, across DMN variants in all subjects, activations were significantly lower for DMN variants than the matched location in other subjects. See *SI Appendix, Fig. S6* for more extended examples.

systems. The second subgroup consisted of individuals whose variants exhibited stronger correlations to the DMN, among others ($N_{MSC} = 4$ of 9, $N_{HCP,1} = 83$ of 192, $N_{HCP,2} = 80$ of 192) (Fig. 5, pink). The 2 subgroups were strongly anticorrelated (see the matrices on the left in Fig. 5), indicating that functional characteristics of variants in these subgroups differed substantially from one another. We observed a similar but weaker pattern of subgroups when individuals were clustered based on the overall size of each functional network relative to the group average (*SI Appendix, Fig. S11*).

Moreover, we observed a small but significant difference between the 2 HCP subgroups in terms of neuropsychological measures of behavior (*SI Appendix, Fig. S12*). We found that individuals in the control and processing subgroup had a higher score [$t(344) = 2.04$, $P < 0.05$] in the positive life-experience factor and a lower score [$t(344) = 2.04$, $P < 0.05$] in the history of drug abuse factor. Both differences were significant after false-discovery rate-correction (see *SI Appendix* for full details).

Jointly, these findings suggest that individuals cluster into subgroups based on the network assignment of each variant, with one subgroup exhibiting more control and processing-like variants and the other subgroup exhibiting more default-like variants. Importantly, these findings provide evidence for systematic

variation of network variants across individuals that replicated across 3 independent samples, with potential implications for behavior.

As noted above, when we examined cluster solutions across alternate thresholds (*Materials and Methods* and *SI Appendix, Fig. S9*), we observed subpatterns within each of the 2 primary clusters in the large HCP samples at lower (sparser) thresholds. There was some evidence for a 4-subgroup solution (*SI Appendix, Fig. S10*), but it was less reliable than the 2-subgroup solution across HCP split-halves. The presence of more fine-grained subgroups suggests that greater sample size, as well as the inclusion of additional measures and data from clinical populations, might yield further clusters of individuals not yet characterized, and potentially more fine-grained relationships between variants and behavior.

Discussion

The present study deepens our understanding of individual differences in the systems-level organization of the human brain by demonstrating that these differences reflect stable, trait-like features with systematic properties that cluster across individuals. Specifically, our results demonstrate that network variants: 1) Show high session-to-session stability in highly sampled

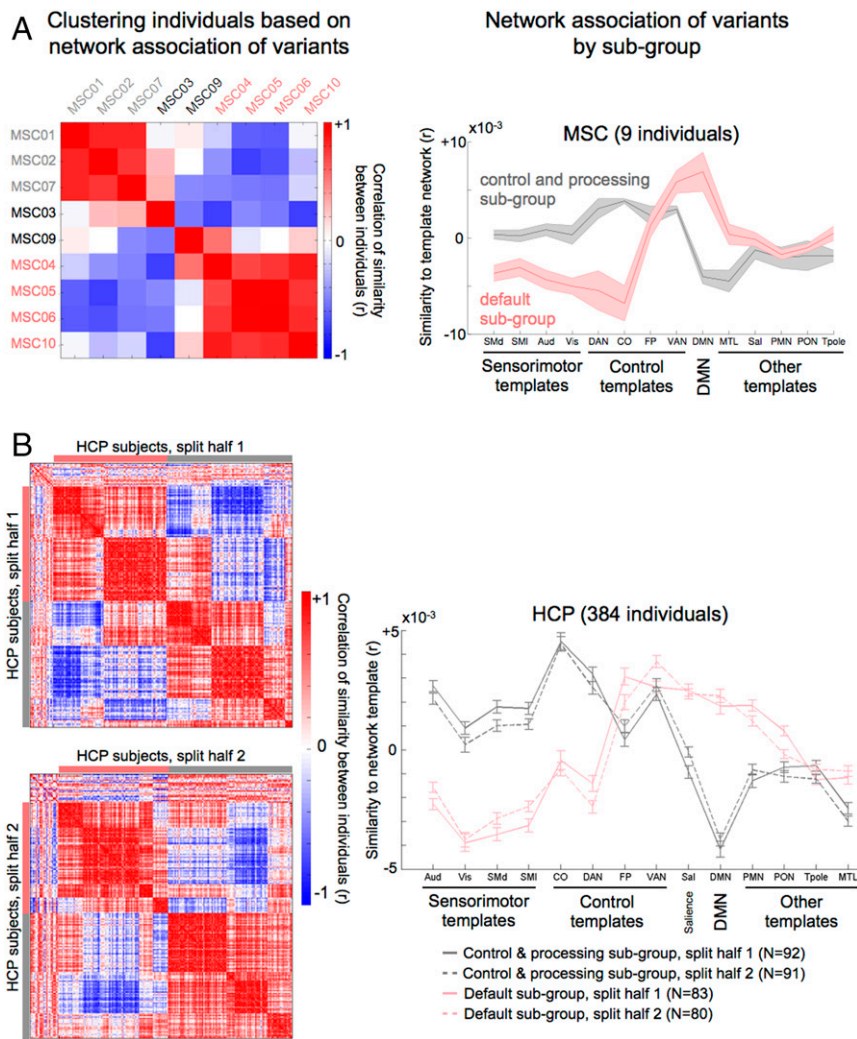


Fig. 5. Separable groups of individuals via network associations of variants. The figure displays groups of individuals in the (A) MSC and (B) HCP datasets clustered by the network associations of their variants. Network associations were computed for each variant as their similarity to templates of 14 canonical functional networks (*Materials and Methods*) (11). The matrices on the left show the correlation between pairs of individuals in terms of variant network associations; each row/column represents a single individual's correlation to all other individuals. The matrices were clustered in a data-driven fashion using InfoMap. The gray and pink colors or bars along the edges of the matrices denote individuals in the same subgroup. These groupings were used to create the averages (line graphs) on the right. The line graphs show the average similarity of variants to each functional network template for individuals within the control and processing subgroup (gray) and the default subgroup (pink; error bars = SEM across individuals).

individuals, suggesting that they are trait-like; 2) occur commonly in lateral frontal and temporoparietal regions and often associate with the DMN, CO, and other control networks, suggesting a systematic linkage to higher-level functions; 3) are related to functional variations during tasks, displaying brain (de-) activations consistent with their novel network reassignment and validating their putative network function; and 4) have a systematic patterning across individuals, allowing for the clustering of individuals into subgroups, with small differences in behavior between subgroups. Jointly, these findings suggest that network variants are promising candidates for endo-phenotypic markers of systems-level brain variability.

Network Variants Are Stable, Trait-Like Components of Individual Functional Brain Organization. Our primary goal was to investigate properties of network variants. We hypothesized that they might show trait-like differences, including stability over time within individuals and systematic variation across individuals.

We found that all individuals across 2 independent datasets (with separate scanners and scan parameters, $n = 393$) showed

characteristic focal deviations from the group-level description of functional brain organization. This indicates that network variants are standard components of typical adult functional network organization, as hinted at by the strong individual variation reported in previous research (10–15). Moreover, we expand upon these findings by showing that network variants are stable within an individual, appearing consistently across 10 independent resting-state fMRI sessions in highly sampled individuals. These findings extend previous evidence that resting-state correlations are sensitive to individual differences in brain organization, given sufficient data and adequate control for nuisance sources of variance (10, 15, 32–34).

Our results also indicate that group-average functional networks represent a mixture of individuals from distinct subgroups (Fig. 5). However, we demonstrate that network variants are highly localized to particular portions of the cortex. In other words, individuals showed substantial similarity to the group-average networks at most cortical locations. Since the maximum spatial overlap of network variants is $\sim 33\%$, the group average may be a reasonable description for the majority of individuals in

most brain locations. Thus, group-average functional networks provide an adequate description of the expected pattern of brain organization, but the group average is not a good representation of any given person and is, therefore, limited in inferences that can be drawn about brain–behavior relationships.

Taken together, the presence of network variants in all individuals and their robustness over sessions provides compelling evidence that they act as stable variations in the systems-level organization of the human brain. These features may prove to be useful substrates in understanding individual differences in brain function and behavior across many domains.

Network Variants Have Characteristic Distributions and Functional Network Associations Across Individuals. We observed that network variants are found commonly near the temporo–occipito–parietal junction and in the lateral prefrontal cortex. We rarely detected network variants in primary sensorimotor cortical areas, the insula, superior parietal lobe, or posterior cingulate cortex. This finding not only replicates across independent datasets, but also converges with previous studies of individual differences in functional network organization reporting high individual differences in association networks (8, 11, 34, 35), with a few specific differences. For example, compared to Mueller et al. (8), we found more network variants near the inferior frontal gyrus and fewer near angular gyrus and supramarginal gyrus. Differences in data processing and registration (surface-based, here) may have contributed to some of these discrepancies. This idea is supported by the similarity of the results here and those reported by Kong et al. (35).

Interestingly, the distribution of common locations for network variants does not appear to be symmetric between the 2 hemispheres, as we found generally more variants in the right hemisphere. Lateralization in the brain is a well-established phenomenon, in terms of both anatomy and function (e.g., refs. 36 and 37), even at the level of individual rsFCs (9). The significance and implications of potential network variant lateralization is a topic for future work to explore.

Furthermore, we found that variants tend to associate with the DMN, CO, and other association networks more often than other functional networks. Networks like the CO and FP network are thought to be important for control functions and performance monitoring (22, 28, 38–41), and the DMN has been proposed to be involved in numerous domains, including autobiographical memory, internal monitoring, and theory of mind (42–44). Network variants occur most often in these “association” networks, and they tend to reassign from one higher-level functional network to another. Together, these results suggest that flexibility in functional network organization may relate more closely to higher-level functions typically associated with these regions.

Network Variants Exhibit Functional Variations during Tasks. We observed that network variants coincide with locations of functional variations during tasks in the MSC dataset. Specifically, we demonstrated that variants that associate with the DMN exhibit decreases in activity during task performance, as has been robustly observed for canonical DMN regions in most externally directed tasks (27). This was the case even in DMN variants in the dorsolateral prefrontal cortex, a brain region that canonically shows robust positive activity during tasks in most individuals. Moreover, this de-activation was not a general property of all variants; variants associated with task-activated systems like the visual, DAN, and FP networks showed (positive) activations. Similarly, CO network variants showed a trend toward higher levels of sustained activation, consistent with a role of the CO network in the stable maintenance of task set (22, 28–30). This finding provides initial validation that network variants shift toward the response characteristics of their functional network assignment during task performance, providing corroborating

evidence that variants reflect true deviations in the functional organization of individual human brains that impact task function.

This result converges with work from Tavor et al. (45), who built a model that was able to predict individual differences in task activations on the basis of individual differences in resting-state data. Their model did not specifically operate on network variants, although the presence of network variants would certainly impact the training of the model. Similarly, Gordon et al. (13) demonstrated that individual specific task-related activation patterns map onto that individual’s resting-state functional networks better than they map onto different individuals’ networks. Here, we build on these findings by showing that network variants specifically show improved task–rest alignment in individuals compared with canonical network assignments. Finally, seminal work from Miller and colleagues revealed stable, meaningful individual differences in brain activations during task performance (1–4). These investigations led to the idea that individual-specific activation patterns reflect, or are potentially determined by, subject-specific information-processing strategies. The results presented herein suggest that if these hypotheses are true, this trait-like brain activity may be localized to network variant regions, specifically.

Individuals Cluster into Discrete Groups on the Basis of Network Variant Characteristics. We found evidence for subgroups of individuals within a normative sample with similar forms of network variants, suggesting that variants demonstrate systematic variation across individuals. Intriguingly, it was the network assignment of variants, rather than their anatomical location, that appeared to be the driving force behind these distinct subgroups. That is, it appears as though group-level variation of network variants is more related to functional assignment than location.

We observed 2 subgroups across individuals that were consistent in both datasets. The 2 subgroups were composed of individuals with more control and processing-like variants and individuals with more default-like variants. The strong distinction between the subgroups may relate to the specific functional networks onto which the variants map, which generally activate and de-activate, respectively, during externally directed tasks (46, 47). A related possibility is that the distinction between the subgroups may be due to changes in the relative size of the aforementioned networks. In other words, individuals with more default-like variants may have an expanded DMN, which could be achieved via “trading” anatomical space canonically occupied by control and processing functional networks for DMN network variants (and vice-versa). Any of these possibilities relates to the trait-like status of the distributions of variants across individuals.

While our work provides initial evidence for groups of individuals with similar network variants across 2 different samples, it appears likely that additional subgroups will be found in future studies. Some additional subgroups may be associated with other properties of network variants (e.g., specific locations, networks, and their interactions), while others may emerge with a more behaviorally diverse range of individuals (e.g., those with neurologic or psychiatric disorders). Notably, in the larger HCP dataset we observed some evidence of further clustering, with the 2 initial groups dividing further into 4 subgroups of individuals. The current work presents a starting point for future investigations into systematic variation in individual functional brain organization, an area that merits substantial additional exploration.

Network Variants May Relate to Behavior. The trait-like nature of network variant distributions raises the question of whether or not network variants relate to individual differences in behavior. It is possible that these individual differences in brain organization reflect different manners of instantiating the same behavior, a behavioral phenocopy (48), or functional degeneracy (49, 50). In other words, network variants may reflect individual differences in processing organization that ultimately lead to

to higher-level cognitive functions. Moreover, network variants are related to functional variations during tasks. Finally, individuals cluster into subgroups on the basis of these variants and these subgroups demonstrate small differences in behavior. Taken in sum, our data support the idea that network variant distributions are trait-like and their patterning across individuals is functionally relevant.

Materials and Methods

Datasets, Acquisition Parameters, and Exclusion Criteria. Three datasets are analyzed in this report: The MSC (13), MyConnectome (24), and HCP (25) datasets. In addition, for group-average comparisons, a previously collected dataset of 120 typical adults was used as the group-level referent (17), referred to in the text as the WashU 120. All data collection was approved by the Washington University and University of Texas Internal Review Boards and all procedures complied with ethical regulations for studies involving human research participants. Dataset composition, acquisition parameters, and exclusion criteria have been described in detail previously (10, 13, 24, 25) for all datasets (see *SI Appendix* for a brief description).

Data and Code Availability. All data and data-processing code used in the manuscript are publicly available (MSC and code: <https://openneuro.org/datasets/ds000224/versions/00002> MyConnectome: myconnectome.org/wp/; HCP: <https://db.humanconnectome.org/app/template/Login.vm>; WashU 120: <https://legacy.openfmri.org/dataset/ds000243/>). Code for network variant analyses (custom MATLAB scripts) are available at <https://github.com/MidnightScanClub>.

Resting-State Data Processing. All data processing has been described in detail previously for each dataset. For extended details, see ref. 13 for MSC, ref. 10 for MyConnectome, ref. 67 for HCP, and ref. 68 for WashU 120. We briefly review relevant details for each type of processing below.

Anatomic processing. First, FreeSurfer 5.3 automatic segmentation was applied to the T1-weighted images to create masks of the gray matter, white matter, and ventricles for each subject (69). Then, FreeSurfer's default recon-all pipeline was used to reconstruct each subject's native anatomical surface. These native surfaces were aligned to the fsaverage surface using a shape-based spherical registration (70–73). The 2 hemispheres were registered to each other using a landmark-based algorithm (74, 75). The final resolution of each subject's surface was 32,492 vertices per hemisphere.

Functional processing. For each subject, standard preprocessing procedures were applied (slice-timing correction, functional realignment, mode 1,000 normalization, atlas registration and resampling, and distortion correction) in addition to further preprocessing to remove motion-related artifacts (frame-wise displacement for frame censoring, regression of nuisance signals, including the whole-brain mean, interpolation over censored frames, and bandpass filtering) (68). See *SI Appendix* for full details.

Volume-to-surface mapping and functional connectivity processing. After preprocessing, a CIFTI was created for each subject. Preprocessed BOLD time series data were mapped to the surface following the procedure of Gordon et al. (76). Before computing the correlations, all previously censored frames were discarded to account for distance-dependent motion artifacts (68). Pairwise correlations between time series from every pair of cortical surface vertices from both hemispheres ($59,412 \times 59,412$) were computed to construct an individual-specific vertex-to-vertex correlation matrix, which was then Fisher-transformed. For the WashU 120 dataset, the individual correlation matrices were averaged together. See *SI Appendix* for full details.

Task Data Processing. In this study, we focus on activations in the 2 mixed design (77) tasks from the MSC dataset: The semantic task and the coherence task. Tasks and their analyses are described in detail in Gordon et al. (13). Task activations were modeled with in-house imaging analysis software (IDL) using a general linear model approach, as previously described (13, 15). See *SI Appendix* for a brief description.

The DMN has been consistently linked to task-deactivations. To determine whether network variants (see next section) associated with the DMN also show the same functional profile, we examined network variant activations in all conditions (cues, trials, and sustained activations) vs. implicit baseline. We conducted this comparison for variants associated with each network, canonical (i.e., nonvariant, group) regions associated with each network, and the average of canonical regions associated with all other networks. In addition, the average activation of each DMN variant in a single individual was compared with the average activation of that same location in other individuals. In all cases, statistical comparisons were carried out using paired 2-sided t tests.

In addition, we added a complementary supplementary analysis of task activations associated with the CO system. The CO network has been consistently linked to sustained activations, especially during resource-limited tasks, unlike other control systems such as the FP network (22, 29, 30). To examine whether variants associated with the CO network displayed sustained activations, we examined activations associated with the sustained block regressor during a resource-limited semantic task (28).

Identification of Network Variants. To identify network variants, individual subject correlation matrices were compared (independently) to a group-average correlation matrix generated from the WashU 120. For each individual, the spatial similarity between the individual's and the group's pattern of correlations (seed map) at each cortical surface vertex was computed. More precisely, each row of an individual's matrix was correlated with the corresponding row in the group-average matrix, resulting in one spatial correlation per vertex. Susceptibility regions were masked out using a vertex-wise measure of signal quality derived from the group-average data. All vertices with a mean BOLD signal less than 750 (as computed in ref. 78) were set to 0. Then, the spatial similarity was binarized such that all cortical vertices with a spatial correlation value in the lowest decile of the individual's distribution were considered for further analyses (these vertices were set to 1, and all others were set to 0). Network variants were defined as regions of the cortex in which sets of at least 50 contiguous vertices were below the spatial correlation threshold. As an alternative to allowing the threshold for network variants to vary across individuals (lowest decile of the individual's spatial correlation distribution), the threshold was fixed at a spatial correlation value of 0.3. Results were extremely consistent between analysis procedures, given that the mean lowest decile cutoff value is 0.32 ± 0.03 .

Functional Network Assignment of Network Variants. A winner-take-all procedure was implemented to assign functional networks to each network variant in each individual. To do so, 14 template networks were created from the 14 group-average networks, as described previously (12). The templates are the group-average resting-state correlation pattern (seed map) of each canonical functional network in the WashU 120 (e.g., the group-average DMN seed map, the group-average visual network seed map, and so forth). Then, for each unique network variant, the following matching procedure was applied: 1) A seed map was computed from the average BOLD time series from all vertices within the network variant; 2) the similarity between that variant seed map and each template network was computed (i.e., the spatial correlation between the template seed map and the variant seed map); 3) the template network with the highest similarity was assigned to the network variant; 4) any network variants where the winning template system had low similarity (i.e., $r < 0.3$) were reassigned as "unknown system"; and finally, 5) we ensured that the variant did not match the group-average network at that cortical location. In other words, we removed the variant if it overlapped (spatially) with its assigned group-average functional network by 50% or more (this occurred infrequently: 5 of 129 = 4% in the MSC dataset, 276 of 7,498 = 3.7% in the HCP dataset).

Overlap of Network Variants Across Individuals. In order to examine the spatial overlap of network variants across individuals, binary versions of the final maps of network variants (after functional network assignment) were summed across individuals to create an overlap map within each dataset. These were divided by the number of people within each dataset, to express the frequency of network variants at each cortical vertex.

Within-Subject Reliability of Network Variants. To measure within-subject reliability of network variants, we compared variants across different days from the same participant. Each MSC subject had 10 independent 30-min resting-state sessions collected on separate days. We processed each session separately (as described above) in order to assess within-subject session-to-session variability of network variants. For each session, we generated the spatial correlation map used for identifying network variants (seed maps from the session vs. seed maps from the group average). Then, we measured the ICC of each map within an individual. In addition, this entire analysis was repeated with binarized network variant maps, but computing the mean dice coefficient instead of ICCs (since the maps are binary). The latter analysis allowed for a focused reliability measure of variant regions only. For the binarized variants analysis, we generated a null model of between-subject variant overlaps for comparison. We performed 1,000 random permutations of pairs of sessions drawn from 2 different MSC individuals (with replacement) and computed the mean dice coefficient of the binary network variant maps from those sessions. For the MyConnectome dataset, we

compared the stability of network variants from sequential 3-wk blocks of data (i.e., variants identified from 6 sessions concatenated together for each 3-wk block). All possible pairs of variant spatial correlation maps (from each 3-wk block of time) were correlated with one another.

Patterns of Network Variants Across Individuals. Next, we turned our attention to whether similar types of network variants were seen across subgroups of individuals. We tested 2 options: 1) Whether subgroups of individuals exhibited variants at similar anatomical locations and, 2) whether subgroups of individuals exhibited variants with similar network associations.

Anatomical. To determine whether subgroups of individuals exhibited variants at similar anatomical locations, we compared the binary maps of (final) network variants between each pair of individuals using dice coefficients. This resulted in a symmetric dice overlap matrix with a size of N by N (9×9 for the MSC dataset and 192×192 for each HCP split-half), with each entry representing the degree to which a given pair of individuals covaries in terms of the spatial distribution of network variants (i.e., the degree to which the pair both have variants 1, 2, and 3 and they both do not have variants 4, 5, and 6). A clustering algorithm (InfoMap) (31) was applied to this dice overlap matrix. Before clustering, we applied a threshold to the matrix to create a sparse network on which to operate. We examined a wide range of density thresholds from the top 2 to 30% of correlations in increments of 1%.

Functional. To determine whether subgroups of individuals exhibited variants with similar network associations, we compared their match to 14 standard network templates. Specifically, during functional network assignment of variants, we compute the similarity (i.e., spatial correlation) between each variant and each template functional network. This results in a 14×1 vector of correlations (to the 14 template networks) for each variant. This measure represents the degree to which a variant is default mode-like, visual-like, and so forth. Then, we computed the variant-size-weighted mean similarity for all variants within an individual to each template network (indicating the degree to which all of that individual's variants are default mode-like, visual-like, and so forth). This mean measure was correlated across subjects, and the same clustering algorithm (InfoMap) was implemented to identify groups of individuals with similar patterns of network variants. We used a range of thresholds from 2 to 10% in increments of 1%.

Conceptually, the functional measure discussed above calculates the average similarity of variants to canonical networks, producing a quantitative estimate of the (for example) DMN-like characteristics of all variants in an

individual. To complement this measure, we also clustered individuals based on the amount of the cortex (number of surface vertices) assigned to each functional network. The WashU 120 group-average functional networks were used as a referent to compare the relative expansion or reduction of each individual's functional networks. Thus, we calculated the number of expanded or contracted surface vertices for each network (relative to the group-average) using the variants' network assignments; for example, a given individual may have +1,000 CO vertices, -75 default mode vertices, and so on.

Analysis of Behavior. Arguably, an important aspect of network variants is their relation to behavior. As a proof-of-concept, and given network variants' distributions and reassignment to association networks, we examined relationships to the HCP behavioral measures (79). We used exploratory factor analysis (EFA) for data reduction and to identify latent constructs in the HCP data. We focused on behavior categories that included multiple instruments or that did not already have summary measures available, which included demographics, cognition, emotion, and substance use variables. Age, sex, and handedness were not considered in the EFA to allow flexibility to include or exclude these variables in analyses of brain-behavior relationships (e.g., as covariates). Data from all HCP subjects ($n = 1,206$) were included in the EFA. EFA factors were then compared across subgroups using multiple linear regression. Details about the results of the EFA and the regression analysis between HCP subgroups of individuals are in *SI Appendix, Supplemental Methods and Fig. S12*.

ACKNOWLEDGMENTS. We thank Joshua S. Siegel and Deanna M. Barch for assistance with the Human Connectome Project data. This research was supported by NIH Grant T32NS073547 (to B.A.S.), NIH Grant F32NS092290 (to C.G.), NIH Grant R01MH118370 (to C.G.), NIH Grant R25MH112473 (to T.O.L.), NIH Grant T32NS047987 (to B.T.K.), National Science Foundation Graduate Research Fellowship Program Award DGE-1143954 (to A.W.G.), an American Psychological Association Dissertation Research Award (to A.W.G.), NIH Grant K01MH104592 (to D.J.G.), a Dart Neuroscience, LLC Grant (to K.B.M.), a McDonnell Foundation Collaborative Activity Award (to S.E.P.), NIH Grant R01NS32979 (to S.E.P.), NIH Grant R01NS06424 (to S.E.P.), and Career Development Award 1K2CX001680 (to E.M.G.) from the US Department of Veterans Affairs Clinical Sciences Research and Development Service. The contents of this manuscript do not represent the views of the US Department of Veterans Affairs or the United States Government.

1. M. B. Miller *et al.*, Unique and persistent individual patterns of brain activity across different memory retrieval tasks. *Neuroimage* **48**, 625–635 (2009).
2. M. B. Miller, C. L. Donovan, C. M. Bennett, E. M. Aminoff, R. E. Mayer, Individual differences in cognitive style and strategy predict similarities in the patterns of brain activity between individuals. *Neuroimage* **59**, 83–93 (2012).
3. J. D. Van Horn, S. T. Grafton, M. B. Miller, Individual variability in brain activity: A nuisance or an opportunity? *Brain Imaging Behav.* **2**, 327–334 (2008).
4. E. Congdon *et al.*, Engagement of large-scale networks is related to individual differences in inhibitory control. *Neuroimage* **53**, 653–663 (2010).
5. M. Neta, P. J. Whalen, Individual differences in neural activity during a facial expression vs. identity working memory task. *Neuroimage* **56**, 1685–1692 (2011).
6. R. Kanai, G. Rees, The structural basis of inter-individual differences in human behaviour and cognition. *Nat. Rev. Neurosci.* **12**, 231–242 (2011).
7. P. A. Filipek *et al.*, Volumetric MRI analysis comparing subjects having attention-deficit hyperactivity disorder with normal controls. *Neurology* **48**, 589–601 (1997).
8. S. Mueller *et al.*, Individual variability in functional connectivity architecture of the human brain. *Neuron* **77**, 586–595 (2013).
9. D. Wang *et al.*, Parcellating cortical functional networks in individuals. *Nat. Neurosci.* **18**, 1853–1860 (2015).
10. T. O. Laumann *et al.*, Functional system and areal organization of a highly sampled individual human brain. *Neuron* **87**, 657–670 (2015).
11. E. M. Gordon, T. O. Laumann, B. Adeyemo, S. E. Petersen, Individual variability of the system-level organization of the human brain. *Cereb. Cortex* **27**, 386–399 (2017).
12. E. M. Gordon *et al.*, Individual-specific features of brain systems identified with resting state functional correlations. *Neuroimage* **146**, 918–939 (2017).
13. E. M. Gordon *et al.*, Precision functional mapping of individual human brains. *Neuron* **95**, 791–807.e7 (2017).
14. R. M. Braga, R. L. Buckner, Parallel interdigitated distributed networks within the individual estimated by intrinsic functional connectivity. *Neuron* **95**, 457–471.e5 (2017).
15. C. Gratton *et al.*, Functional brain networks are dominated by stable group and individual factors, not cognitive or daily variation. *Neuron* **98**, 439–452.e5 (2018).
16. S. Marek *et al.*, Spatial and temporal organization of the individual human cerebellum. *Neuron* **100**, 977–993.e7 (2018).
17. J. D. Power *et al.*, Functional network organization of the human brain. *Neuron* **72**, 665–678 (2011).
18. B. T. T. Yeo *et al.*, The organization of the human cerebral cortex estimated by intrinsic functional connectivity. *J. Neurophysiol.* **106**, 1125–1165 (2011).
19. B. Biswal, F. Z. Yetkin, V. M. Haughton, J. S. Hyde, Functional connectivity in the motor cortex of resting human brain using echo-planar MRI. *Magn. Reson. Med.* **34**, 537–541 (1995).
20. D. Cordes *et al.*, Mapping functionally related regions of brain with functional connectivity MR imaging. *AJNR Am. J. Neuroradiol.* **21**, 1636–1644 (2000).
21. M. J. Lowe, B. J. Mock, J. A. Sorenson, Functional connectivity in single and multislice echoplanar imaging using resting-state fluctuations. *Neuroimage* **7**, 119–132 (1998).
22. N. U. F. Dosenbach *et al.*, Distinct brain networks for adaptive and stable task control in humans. *Proc. Natl. Acad. Sci. U.S.A.* **104**, 11073–11078 (2007).
23. S. M. Smith *et al.*, Correspondence of the brain's functional architecture during activation and rest. *Proc. Natl. Acad. Sci. U.S.A.* **106**, 13040–13045 (2009).
24. R. A. Poldrack *et al.*, Long-term neural and physiological phenotyping of a single human. *Nat. Commun.* **6**, 8885 (2015).
25. D. C. Van Essen *et al.*; WU-Minn HCP Consortium, The Human Connectome Project: A data acquisition perspective. *Neuroimage* **62**, 2222–2231 (2012).
26. T. O. Laumann *et al.*, On the stability of BOLD fMRI correlations. *Cereb. Cortex* **27**, 4719–4732 (2017).
27. G. L. Shulman *et al.*, Common blood flow changes across visual tasks: II. Decreases in cerebral cortex. *J. Cogn. Neurosci.* **9**, 648–663 (1997).
28. J. W. Dubis, J. S. Siegel, M. Neta, K. M. Visscher, S. E. Petersen, Tasks driven by perceptual information do not recruit sustained BOLD activity in cingulo-opercular regions. *Cereb. Cortex* **26**, 192–201 (2016).
29. N. U. F. Dosenbach *et al.*, A core system for the implementation of task sets. *Neuron* **50**, 799–812 (2006).
30. N. U. F. Dosenbach, D. A. Fair, A. L. Cohen, B. L. Schlaggar, S. E. Petersen, A dual-network architecture of top-down control. *Trends Cogn. Sci.* **12**, 99–105 (2008).
31. M. Rosvall, C. T. Bergstrom, Maps of random walks on complex networks reveal community structure. *Proc. Natl. Acad. Sci. U.S.A.* **105**, 1118–1123 (2008).
32. U. Braun *et al.*, Test-retest reliability of resting-state connectivity network characteristics using fMRI and graph theoretical measures. *Neuroimage* **59**, 1404–1412 (2012).
33. R. M. Birn *et al.*, The effect of scan length on the reliability of resting-state fMRI connectivity estimates. *Neuroimage* **63**, 550–558 (2013).
34. B. Chen *et al.*, Individual variability and test-retest reliability revealed by ten repeated resting-state brain scans over one month. *PLoS One* **10**, e0144963 (2015).
35. R. Kong *et al.*, Spatial topography of individual-specific cortical networks predicts human cognition, personality, and emotion. *Cereb. Cortex* **29**, 2533–2551 (2019).
36. P. Broca, Remarques sur le siège de la faculté du langage articulé, suivies d'une observation d'aphémie (perte de la parole). *Bull la Société Anat* **6**, 330–357 (1861).

37. R. W. Sperry, Cerebral organization and behavior: The split brain behaves in many respects like two separate brains, providing new research possibilities. *Science* **133**, 1749–1757 (1961).
38. W. W. Seeley *et al.*, Dissociable intrinsic connectivity networks for salience processing and executive control. *J. Neurosci.* **27**, 2349–2356 (2007).
39. S. Sadaghiani, M. D'Esposito, Functional characterization of the cingulo-opercular network in the maintenance of tonic alertness. *Cereb. Cortex* **25**, 2763–2773 (2015).
40. M. Neta, B. L. Schlaggar, S. E. Petersen, Separable responses to error, ambiguity, and reaction time in cingulo-opercular task control regions. *Neuroimage* **99**, 59–68 (2014).
41. C. Gratton *et al.*, Distinct stages of moment-to-moment processing in the cingulo-opercular and frontoparietal networks. *Cereb. Cortex* **27**, 2403–2417 (2017).
42. R. L. Buckner, J. R. Andrews-Hanna, D. L. Schacter, The brain's default network: Anatomy, function, and relevance to disease. *Ann. N. Y. Acad. Sci.* **1124**, 1–38 (2008).
43. R. N. Spreng, R. A. Mar, A. S. N. Kim, The common neural basis of autobiographical memory, prospection, navigation, theory of mind, and the default mode: A quantitative meta-analysis. *J. Cogn. Neurosci.* **21**, 489–510 (2009).
44. M. E. Raichle, The brain's default mode network. *Annu. Rev. Neurosci.* **38**, 433–447 (2015).
45. I. Tavor *et al.*, Task-free MRI predicts individual differences in brain activity during task performance. *Science* **352**, 216–220 (2016).
46. M. D. Fox *et al.*, The human brain is intrinsically organized into dynamic, anticorrelated functional networks. *Proc. Natl. Acad. Sci. U.S.A.* **102**, 9673–9678 (2005).
47. D. S. Margulies *et al.*, Situating the default-mode network along a principal gradient of macroscale cortical organization. *Proc. Natl. Acad. Sci. U.S.A.* **113**, 12574–12579 (2016).
48. B. L. Schlaggar, B. D. McCandliss, Development of neural systems for reading. *Annu. Rev. Neurosci.* **30**, 475–503 (2007).
49. G. Tononi, O. Sporns, G. M. Edelman, Measures of degeneracy and redundancy in biological networks. *Proc. Natl. Acad. Sci. U.S.A.* **96**, 3257–3262 (1999).
50. K. J. Friston, C. J. Price, Degeneracy and redundancy in cognitive anatomy. *Trends Cogn. Sci.* **7**, 151–152 (2003).
51. S. M. Smith *et al.*, A positive-negative mode of population covariation links brain connectivity, demographics and behavior. *Nat. Neurosci.* **18**, 1565–1567 (2015).
52. J. D. Bijsterbosch *et al.*, The relationship between spatial configuration and functional connectivity of brain regions. *eLife* **7**, e32992 (2018).
53. E. S. Finn *et al.*, Functional connectome fingerprinting: Identifying individuals using patterns of brain connectivity. *Nat. Neurosci.* **18**, 1664–1671 (2015).
54. R. J. Tusa, L. A. Palmer, A. C. Rosenquist, "Multiple cortical visual areas" in *Multiple Visual Areas*, C. N. Woolsey, Ed. (Cortical Sensory Organization, Humana Press, 1981), vol. 2, pp. 1–31.
55. R. M. Bowker, J. D. Coulter, "Intracortical connectivities of somatic sensory and motor areas" in *Multiple Somatic Areas*, C. N. Woolsey, Ed. (Cortical Sensory Organization, Humana Press, 1981), vol. 1, pp. 205–242.
56. J. F. Brugge, "Auditory cortical areas in primates" in *Multiple Auditory Areas*, C. N. Woolsey, Ed. (Cortical Sensory Organization, Humana Press, 1982), vol. 3, pp. 59–70.
57. R. F. Dougherty *et al.*, Visual field representations and locations of visual areas V1/2/3 in human visual cortex. *J. Vis.* **3**, 586–598 (2003).
58. H. J. Park *et al.*, Morphological alterations in the congenital blind based on the analysis of cortical thickness and surface area. *Neuroimage* **47**, 98–106 (2009).
59. J. Jiang *et al.*, Thick visual cortex in the early blind. *J. Neurosci.* **29**, 2205–2211 (2009).
60. U. Noppeney, K. J. Friston, J. Ashburner, R. Frackowiak, C. J. Price, Early visual deprivation induces structural plasticity in gray and white matter. *Curr. Biol.* **15**, R488–R490 (2005).
61. K. M. Bishop, G. Goudreau, D. D. M. O'Leary, Regulation of area identity in the mammalian neocortex by Emx2 and Pax6. *Science* **288**, 344–349 (2000).
62. T. Hamasaki, A. Leingärtner, T. Ringstedt, D. D. M. O'Leary, EMX2 regulates sizes and positioning of the primary sensory and motor areas in neocortex by direct specification of cortical progenitors. *Neuron* **43**, 359–372 (2004).
63. M. F. Glasser *et al.*, A multi-modal parcellation of human cerebral cortex. *Nature* **536**, 171–178 (2016).
64. T. Paus, Location and function of the human frontal eye-field: A selective review. *Neuropsychologia* **34**, 475–483 (1996).
65. E. J. Tehovnik, M. A. Sommer, I. H. Chou, W. M. Slocum, P. H. Schiller, Eye fields in the frontal lobes of primates. *Brain Res. Brain Res. Rev.* **32**, 413–448 (2000).
66. M. J. Arcaro, P. F. Schade, J. L. Vincent, C. R. Ponce, M. S. Livingstone, Seeing faces is necessary for face-domain formation. *Nat. Neurosci.* **20**, 1404–1412 (2017).
67. M. F. Glasser *et al.*; WU-Minn HCP Consortium, The minimal preprocessing pipelines for the Human Connectome Project. *Neuroimage* **80**, 105–124 (2013).
68. J. D. Power *et al.*, Methods to detect, characterize, and remove motion artifact in resting state fMRI. *Neuroimage* **84**, 320–341 (2014).
69. B. Fischl *et al.*, Whole brain segmentation: Automated labeling of neuroanatomical structures in the human brain. *Neuron* **33**, 341–355 (2002).
70. A. M. Dale, B. Fischl, M. I. Sereno, Cortical surface-based analysis. I. Segmentation and surface reconstruction. *Neuroimage* **9**, 179–194 (1999).
71. B. Fischl, M. I. Sereno, A. M. Dale, Cortical surface-based analysis. II: Inflation, flattening, and a surface-based coordinate system. *Neuroimage* **9**, 195–207 (1999).
72. A. M. Dale, M. I. Sereno, Improved localization of cortical activity by combining EEG and MEG with MRI cortical surface reconstruction: A linear approach. *J. Cogn. Neurosci.* **5**, 162–176 (1993).
73. F. Ségonne, E. Grimson, B. Fischl, A genetic algorithm for the topology correction of cortical surfaces. *Inf. Process. Med. Imaging* **19**, 393–405 (2005).
74. A. Anticevic *et al.*, Automated landmark identification for human cortical surface-based registration. *Neuroimage* **59**, 2539–2547 (2012).
75. D. C. Van Essen, M. F. Glasser, D. L. Dierker, J. Harwell, T. Coalson, Parcellations and hemispheric asymmetries of human cerebral cortex analyzed on surface-based atlases. *Cereb. Cortex* **22**, 2241–2262 (2012).
76. E. M. Gordon *et al.*, Generation and evaluation of a cortical area parcellation from resting-state correlations. *Cereb. Cortex* **26**, 288–303 (2016).
77. S. E. Petersen, J. W. Dubis, The mixed block/event-related design. *Neuroimage* **62**, 1177–1184 (2012).
78. J. G. Ojemann *et al.*, Anatomic localization and quantitative analysis of gradient-reduced echo-planar fMRI susceptibility artifacts. *Neuroimage* **6**, 156–167 (1997).
79. D. M. Barch *et al.*; WU-Minn HCP Consortium, Function in the human connectome: Task-fMRI and individual differences in behavior. *Neuroimage* **80**, 169–189 (2013).